

Zeno crossovers in the entanglement speed of spin chains with noisy impurities

Abhijit P. Chaudhari,¹ Shane P. Kelly,² Riccardo Javier Valencia Tortora,² and Jamir Marino²

¹*Department of Physics, Indian Institute of Technology (Banaras Hindu University), Varanasi - 221005, India**

²*Institut für Physik, Johannes Gutenberg Universität Mainz, D-55099 Mainz, Germany*

(Dated: March 1, 2025)

We study a one dimensional quantum XY spin chain driven by a local noisy spin impurity with finite correlation time, along the transverse field direction. We recover the celebrated Zeno crossover and we show that entanglement can be used as a proxy for the heating and strong-measurement regimes. We compute the entanglement entropy of a block of spins and we observe that its velocity of spreading decreases at strong dissipation, as a result of the Zeno effect. Upon increasing the correlation time of the noise, the location of the Zeno crossover shifts at stronger dissipation rates opening up a broader heating phase. We offer insight on the mechanisms underlying the dynamics of the entanglement entropy by monitoring different time traces of the local transverse magnetisation profile. Our results aim at starting a complementary viewpoint on the field of dissipative quantum impurities, based on a theoretical quantum information perspective.

I. INTRODUCTION

Impurity models represent a traditional avenue [1, 2] for developing intuition in complex many-body problems ranging from condensed matter physics to solid state and encompassing cold atoms. A recent line of investigation is extensively revisiting instances of prototypical impurity systems in a dissipative setting, with the aim to provide future guidance in the solution of the driven-dissipative quantum many-body problem. The effect of a localised dissipative potential can be implemented, for instance, by shining an electron beam on an atomic BEC [3, 4], and it results in a decrease of atom losses at strong dissipation rate. This is a manifestation of a many-body version of the Zeno effect [5–10], where the usual slowdown of transport at strong measurement is at interplay with many-particle correlation effects [11]. Furthermore, losses provided by a near-resonant optical tweezer at a quantum point contact, can realise a dissipative scanning gate microscope for ultra-cold ⁶Li atoms [12, 13], offering a resource for transport problems. At the same time, like in their unitary counterparts, dissipative impurities can also have an intrusive effect and significantly rearrange the properties of many-body states as in the Anderson impurity problem [2, 14]. A classification of the phenomenology of dissipative impurities is currently subject of vivid research at the interface of quantum information, atomic physics, quantum optics and solid state [15–22]; it comprises driven-dissipative boundary spin problems [23–29], and the realisation of the many-particle Zeno effect in lossy (and noisy) condensed matter systems and cold atoms [30–35].

The onset of the Zeno effect is marked by strong suppression of dynamical observables (such as decay rates or currents) beyond a certain dissipation strength. In this work, we take one step further and we inspect whether entanglement quantifiers can expose the Zeno crossover.

By Zeno crossover, we refer to a transition from facilitation to suppression of transport in the wire. It generically occurs upon tuning the strength of noise above the characteristic energy scale of the system as reported in [36] and [30]. Specifically, we consider an exactly solvable instance of the problem, extending previous results on locally noise-driven free fermions [36], to evaluate the entanglement entropy of a block of spins. The Gaussian nature of the problem allows to average over several stochastic realisations, and to follow dynamics for long times and large system sizes, and we show that the growth rate of the entanglement entropy carries a hallmark of the Zeno transition. Our results have the potential to bridge the growing field of dissipative impurities in condensed matter systems with theoretical quantum information science, and stimulate a new line of investigation at their interface.

II. MODEL

We study the quantum XY spin chain [37]

$$H_0 = \sum_{i=-L}^L -(1+\gamma)\sigma_i^x\sigma_{i+1}^x - (1-\gamma)\sigma_i^y\sigma_{i+1}^y - h\sigma_i^z, \quad (1)$$

where σ_i^α , ($\alpha = x, y, z$) are the Pauli matrices for the i^{th} spin along the direction α , and $0 \leq \gamma \leq 1$. The system is considered to be periodic ($\sigma_i^{x,y,z} = \sigma_{2L+1+i}^{x,y,z}$). However the results for the dynamics obtained here are equally valid regardless of boundary condition, as they apply to the bulk of the system. At $t = 0$, the system is prepared in the ground state of H_0 and at subsequent times, we suddenly turn on a time varying stochastic field which drives the spin impurity at the site $i = 0$. The resulting dynamics is given by the time dependent Hamiltonian:

$$H(t) = H_0 + \sqrt{\kappa}\eta(t)\sigma_0^z. \quad (2)$$

The time varying stochastic field $\eta(t)$ is an Ornstein-Uhlenbeck (OU) process [38] with $\langle \eta(t_1)\eta(t_2) \rangle =$

* apraavin.chaudhari.phy16@iitbhu.ac.in

$\exp\left(-\frac{|t_1-t_2|}{\tau}\right)/\tau$. When $\tau \rightarrow 0$, $\eta(t)$ is equivalent to Gaussian white noise. For most of the paper, and unless otherwise stated, we will work in this limit. The main exception is in Sec. IV C, where we study the effects of finite time correlation. The stochastic Schrodinger equation (SSE) with the Hamiltonian in Eq. (2) then reads

$$\partial_t |\psi^\eta(t)\rangle = -iH(t)|\psi^\eta(t)\rangle, \quad (3)$$

where $|\psi^\eta(t)\rangle$ represents the state of the system for a given noise realisation. In the Gaussian white noise limit, the stochastic Schrodinger equation implies the following Linblad evolution [39]

$$\partial_t \rho(t) = -i[\hat{H}_0, \rho(t)] + \frac{\kappa}{2}[\sigma_0^z, [\rho(t), \sigma_0^z]], \quad (4)$$

where $\rho(t) = \langle \rho^\eta(t) \rangle_\eta = \langle |\psi^\eta(t)\rangle \langle \psi^\eta(t)| \rangle_\eta$ is the noise averaged density matrix, and $\langle \dots \rangle_\eta$ represents noise averaging.

In this paper, we study both average properties of stochastic evolution captured by $\rho(t)$, and also more detailed information about the fluctuations of $\rho^\eta(t)$. To elucidate the difference, let us consider a general functional O of $\rho^\eta(t)$. In the case that O is linear in ρ^η (for example, the local magnetisation is given by $O[\rho^\eta] := \text{Tr}[\rho^\eta(t)\sigma_i^z]$), then

$$\langle O[\rho^\eta] \rangle_\eta = O[\rho]. \quad (5)$$

However, when O is non-linear in ρ^η (for example, von-Neumann entropy is given as, $O[\rho^\eta] := -\text{Tr}[\rho^\eta \log_2[\rho^\eta]]$), then

$$\langle O[\rho^\eta] \rangle_\eta \neq O[\rho], \quad (6)$$

in general. Hence, the dynamics of $\langle O[\rho^\eta] \rangle_\eta$ can be significantly different from that of $O[\rho]$. We explore the linear case in Sec. III and the nonlinear case in Sec. IV A.

We study the dynamics of this system using exact simulation methods, and to execute these simulations efficiently, we employ Jordan-Wigner transformation [37] to map $\hat{H}(t)$ to a system of non-interacting spinless fermions:

$$\begin{aligned} \hat{H}(t) = & \sum_{i=-L}^L -(c_i^\dagger c_{i+1} + c_{i+1}^\dagger c_i) + (c_i c_{i+1}^\dagger + c_{i+1} c_i^\dagger) - \gamma(c_i^\dagger c_{i+1}^\dagger + c_{i+1} c_i) + \gamma(c_{i+1}^\dagger c_i^\dagger + c_i c_{i+1}) \\ & - h(c_i c_i^\dagger - c_i^\dagger c_i) - \sqrt{\kappa}\eta(t)(c_0 c_0^\dagger - c_0^\dagger c_0) \\ & + U_p[(c_L^\dagger c_{-L} + c_{-L}^\dagger c_L) - (c_L c_{-L}^\dagger + c_{-L} c_L^\dagger)] + U_p\gamma[(c_L^\dagger c_{-L}^\dagger + c_{-L} c_L) - (c_{-L}^\dagger c_L^\dagger + c_L c_{-L})]. \end{aligned} \quad (7)$$

Under this map, the periodic boundary condition of the spin chain map to a boundary term $2U_p[(c_L^\dagger c_{-L} + c_{-L}^\dagger c_L) + \gamma(c_L^\dagger c_{-L}^\dagger + c_{-L} c_L)]$, where $U_p = \prod_{m=-L}^L \sigma_m^z$ is the parity operator. U_p is known to be a symmetry of $\hat{H}(t)$ [37], and this gives $\hat{H}(t)$ a block diagonal structure in fermionic basis (c_i, c_i^\dagger) . Each block is specified by the eigenvalue ± 1 of U_p . The block corresponding to $+1$ is known as the even sector of $\hat{H}(t)$ and similarly the block corresponding to -1 is known as the odd sector of $\hat{H}(t)$. However, the boundary term does not have any quantitative effects on the bulk properties when L is large enough. Therefore, we can arbitrarily choose one of the sectors for $L \gg 1$. For the purpose of numerical simulations, we consider the even sector and we fix $L \geq 100$.

In addition to numerical efficiency, the Jordan Wigner transformation reveals the nature of the quasi-particle

excitation of the Hamiltonian. To see this, we use a vectorial notation:

$$\mathbf{c} = \begin{pmatrix} c_{-L} \\ \vdots \\ c_L \end{pmatrix}, \bar{\mathbf{c}} = \begin{pmatrix} \mathbf{c} \\ \mathbf{c}^\dagger \end{pmatrix}, \quad (8)$$

$\hat{H}(t)$ can be expressed as

$$\hat{H}(t) = \bar{\mathbf{c}}^\dagger (M_0 + \sqrt{\kappa}\eta(t)\mathcal{L})\bar{\mathbf{c}}. \quad (9)$$

M_0 is the single particle Hamiltonian associated with the coherent part H_0 from $H(t)$ and \mathcal{L} represents the noise term σ_0^z from $H(t)$ [40],

$$M_0 = \begin{bmatrix} \alpha & -\beta \\ \beta & -\alpha \end{bmatrix}, \quad \mathcal{L} = \begin{bmatrix} -\mathbf{L} & 0 \\ 0 & \mathbf{L} \end{bmatrix}, \quad (10)$$

and the matrix elements read

$$\begin{aligned} \alpha_{i,j} &= -(\delta_{i,j+1} + \delta_{i,j-1} - \delta_{i,-L}\delta_{j,L} - \delta_{i,L}\delta_{j,-L}) + h\delta_{i,j}, \\ \beta_{i,j} &= \gamma(\delta_{i,j+1} - \delta_{i,j-1} + \delta_{i,-L}\delta_{j,L} - \delta_{i,L}\delta_{j,-L}), \\ \mathbf{L}_{i,j} &= \delta_{i,0}\delta_{j,0}, \end{aligned} \quad (11)$$

with $i, j \in [-L, L]$. The matrix α captures the hopping of fermions throughout the chain, while β encodes superconducting-like ‘pairing’. Terms like $\beta_{ji}^* c_j^\dagger c_i^\dagger$ and $\beta_{ij} c_i c_j$ create/destroy spinless fermions in pairs akin to analogue terms occurring in the mean field BCS of superconductors [41]. Since $H(t)$ is Hermitian, this implies $\alpha^T = \alpha$ and $\beta^T = -\beta$.

Under the Jordan Wigner transform, the local impurity $\eta(t)\sigma_0^z$ transforms to a noise field coupled to the density of Jordan-Wigner fermions at site zero [36],

$$\eta(t)\sigma_0^z = \eta(t)(1 - 2\hat{n}_0) \quad (12)$$

$$= \eta(t)(1 - 2c_0^\dagger c_0). \quad (13)$$

To better understand the effect of this impurity on dynamics, we identify the natural quasi-particle excitations of H_0 using the standard procedure outlined as follows. First we move to Fourier space using the following definition

$$c_q = \frac{1}{\sqrt{(2L+1)}} \sum_{j=-L}^L c_j e^{iqj}, \quad (14)$$

$$\sigma_0^z = 1 - \frac{2}{2L+1} \sum_{p,q} c_p^\dagger c_q = 1 - \frac{2}{2L+1} \sum_{p,q} -iu_q v_p b_{-p} b_q + iu_p v_q b_p^\dagger b_{-q}^\dagger + v_p v_q b_{-p} b_{-q}^\dagger + u_q u_p b_p^\dagger b_q. \quad (19)$$

This representation of σ_0^z contains several other nontrivial terms in addition to fermion density. When $\gamma = 0$, it is clearly seen that the noise acts as a local dephasing channel. However, when $\gamma \neq 0$, Eq. (19) shows that σ_0^z does not simply act as a local dephasing in Bogoliubov basis, but also contains two body losses and pumps processes ($b_{-p} b_q$ and $b_p^\dagger b_{-q}^\dagger$, respectively) for any non-zero γ . This sets our work apart from the pre-existing literature where localised losses, gains or only dephasing are considered individually.

followed by a Bogoliubov rotation [37, 41, 42]

$$c_q = u_q b_q + i v_q b_{-q}^\dagger \quad (15)$$

$$c_{-q}^\dagger = u_q b_{-q}^\dagger + i v_q b_q, \quad (16)$$

where $u_q = \cos(\theta_q/2)$ and $v_q = \sin(\theta_q/2)$, and θ_q is the $O(2)$ rotation angle for a given mode q

$$\tan \theta_q = \frac{2\gamma \sin q}{h - 2 \cos q}. \quad (17)$$

This overall procedure diagonalises H_0 , such that it takes the following form in (b_q, b_q^\dagger) basis

$$H_0 = \sum_q \epsilon(q) \left(b_q^\dagger b_q - \frac{1}{2} \right), \quad (18)$$

where $\epsilon(q) = -4((\cos(q) + \frac{h}{2})^2 + (\gamma \sin(q))^2)^{\frac{1}{2}}$. In this basis, σ_0^z takes the form

III. PRE-RELAXATION DYNAMICS

In this section we study local magnetisation profile and the global magnetisation of the spin chain. We first evaluate the dynamics of the local magnetisation, $m(i, \gamma, t) = \langle \sigma_i^z(t) \rangle$, as a function of its position along the chain, $i \in [-L, L]$, and time t for different γ . We study the dynamics of the local magnetisation by simulating the adjoint master equation, which takes the following form (given that the jump operator is Hermitian)

$$\begin{aligned} \partial_t \langle \hat{A} \rangle &= \partial_t (\text{Tr}(\hat{A} \rho(t))) \\ &= i \langle [H_0, \hat{A}] \rangle + \frac{\kappa}{2} \langle [\sigma_0^z, [\hat{A}, \sigma_0^z]] \rangle. \end{aligned}$$

This equation gives the equations of motions for the two point correlators, $C_{i,j} = \langle c_i^\dagger(t) c_j(t) \rangle$ and $F_{i,j} = \langle c_i^\dagger(t) c_j^\dagger(t) \rangle$:

$$\partial_t \mathcal{C} = -i[M_0, \mathcal{C}] - 2\kappa \begin{bmatrix} -\mathbf{LC} - \mathbf{CL} + 2\mathbf{LCL} & \mathbf{LF}^\dagger + \mathbf{F}^\dagger \mathbf{L} + 2\mathbf{LF}^\dagger \mathbf{L} \\ \mathbf{LF} + \mathbf{FL} + 2\mathbf{LFL} & \mathbf{LC} + \mathbf{CL} - 2\mathbf{LCL} \end{bmatrix} \quad (20)$$

where \mathcal{C} is constructed such that it contains C and F matrices as follows

$$\mathcal{C} = \begin{bmatrix} \hat{1} - C & F^\dagger \\ F & C \end{bmatrix}. \quad (21)$$

$\hat{1}$ is an identity matrix of size $(2L+1) \times (2L+1)$. The elements of above mentioned matrix are matrices of size $(2L+1) \times (2L+1)$ such that $\mathcal{C}(t)$ is a matrix of size

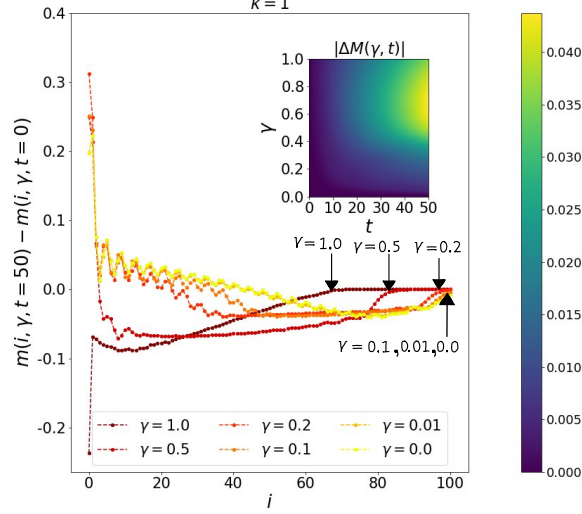


FIG. 1: Local magnetisation with reference to its initial value, as a function of i and t . For all values of γ , we see a ballistic density front emitted by the impurity (shown by black arrows). For small γ (such as $\gamma = 0.01$), the local magnetisation profile does not differ appreciably from the profile obtained for $\gamma = 0$. This similarity fades away as γ increases and reaches its maximum value. The inset shows a density plot of absolute value of the global magnetisation ($M(\gamma, t)$) with reference to its initial value ($\Delta M(\gamma, t) = M(\gamma, t) - M(\gamma, 0)$), with the magnitude increasing from dark to light region. The system appreciably realises the effect of the breaking of rotational invariance along \hat{z} , after a time scale $t \sim 1/\gamma$. The results obtained here are obtained via numerical simulation of adjoint master equation (20). For the results presented here, $L = 100$ and $h = \sqrt{2}$.

$2(2L+1) \times 2(2L+1)$. The local magnetisation is straightforwardly computed via $m(i, \gamma, t) = 1 - 2C_{i,i}(\gamma, t)$ and is presented in Fig. 1.

The stochastic impurity locally perturbs the chain which results in emission of pairs of Bogoliubov quasi-particles. They move with a velocity $v_q = \partial_q \epsilon(q)$, where $\epsilon(q) = -4((\cos(q) + \frac{h}{2})^2 + (\gamma \sin(q))^2)^{\frac{1}{2}}$ (see for instance [42, 43]). This gives rise to a ballistic density front which can be seen in Fig. 1. We observe that the speed of the ballistic density front reduces as γ increases (see Fig. 1). This slowing down of the ballistic density front follows from the group velocity expression [42, 43], (cf. with the expression for $\epsilon(q)$)

$$v_q = 4 \sin(q) \left(\frac{(1 - \gamma^2) \cos(q) + \frac{h}{2}}{\sqrt{(\cos(q) + \frac{h}{2})^2 + \gamma^2 \sin^2(q)}} \right). \quad (22)$$

An increase in γ leads to reduction of group velocity $|v_q|$ for any value of q and h . This implies that $|v_q^{max}|$ decreases as γ increases, confirming our earlier observation. Increasing γ also changes the spatial oscillations that occur before the ballistic density front. We generally observe an amplification of oscillations and, in Fig. 1 show a reduction in the spatial extent of the oscillations for $\gamma > 0$.

When $\gamma = 0$, the system is invariant under rotations along the \hat{z} -axis and as a consequence, the global mag-

netisation ($M(\gamma, t) = \sum_i m(i, \gamma, t)/(2L+1)$) along \hat{z} remains conserved. However, this symmetry is broken for $\gamma \neq 0$ and hence to understand the effects of this symmetry breaking on the dynamics quantitatively, we calculate the difference between the global magnetisation and its initial value (See the inset in Fig. 1). Despite the fact that for $\gamma \neq 0$ the global magnetization along \hat{z} is not conserved, we observe that $M(\gamma, t)$ does not change appreciably as compared to its initial value $M(\gamma, 0)$ up to time scales of the order of $1/\gamma$. This phenomenon happens in a fashion reminiscent of ‘pre-relaxation’ effects in integrable systems [44, 45].

IV. ENTANGLEMENT ENTROPY AS A PROBE OF THE ZENO CROSSOVER

A. Observables and simulation methods

As mentioned in the previous section, the stochastic drive emits entangled pairs of quasi-particles leading to the generation of entanglement [46]. Hence, we turn our attention to the resultant entanglement dynamics. We use the von-Neumann entropy of the reduced density matrix (EE) to quantify entanglement for the block $[x_1, x_2]$

$$S_{ent}^\eta(t) = -\text{Tr}[\rho_{[x_1, x_2]}^\eta \log_2 \rho_{[x_1, x_2]}^\eta], \quad (23)$$

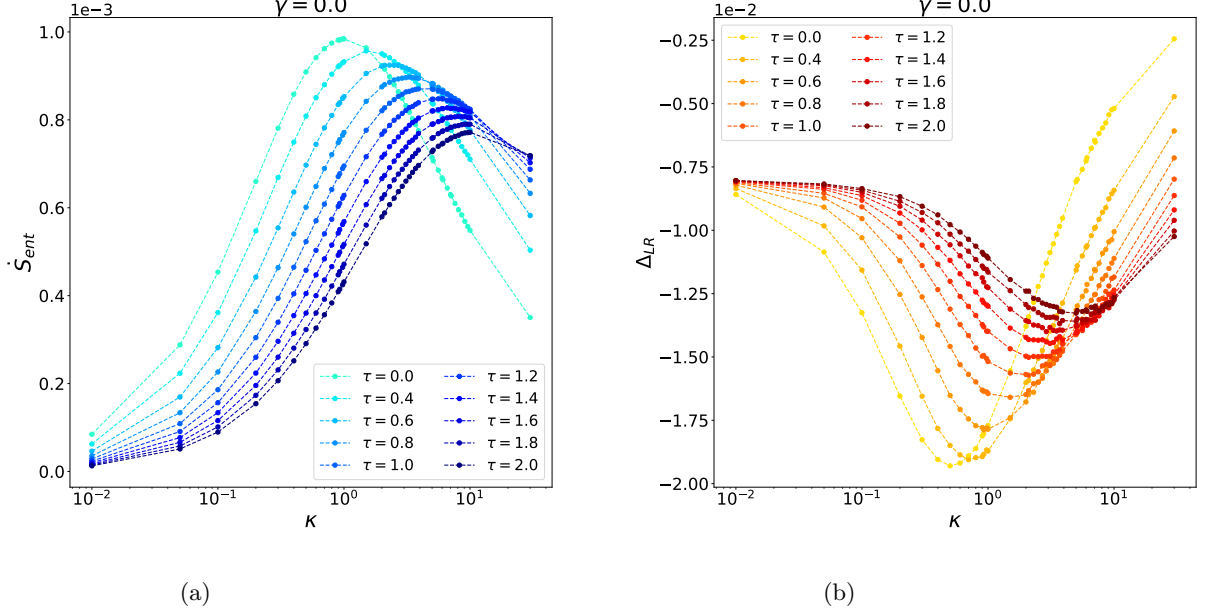


FIG. 2: (a) Velocity of entanglement spreading $\dot{S}_{ent} = \partial_t \langle S^\eta(t) \rangle_\eta$ as a function of coupling to the stochastic field κ and (b) correlation function $\Delta_{LR} = \langle \Delta_{LR}^\eta \rangle_\eta$ as a function of κ , in the long time limit. \dot{S}_{ent} and Δ_{LR} show a Zeno-crossover in the late time limit. For both quantities, we observe that the Zeno crossover occurs at larger values of κ , as the noise correlation time τ increases. The results presented here are obtained via numerical simulation of stochastic Schrodinger equation (3) for $L = 160$ and $h = \sqrt{2}$. They are averaged over $N_\eta = 1.1 \times 10^4$ noise realisations. For the purposes of numerics, we terminate the simulations when $t \sim (2L + 1)/4$. The latter is the smallest time scale at which finite size effects start to appear

where $\rho_{[x_1, x_2]}^\eta$ is, for a given noise realization η , the reduced density matrix $\text{Tr}_{[x_1, x_2]^c}[\rho^\eta]$, on the segment $[x_1, x_2]$, while $\text{Tr}_{[x_1, x_2]^c}$ refers to trace over the remainder of the chain. For the rest of the paper, we will be interested in the noise average of this quantity $\langle S_{ent}^\eta(t) \rangle_\eta$. Our choice to study $\langle S_{ent}^\eta(t) \rangle_\eta$ instead of $S_{ent} = -\text{Tr}[\rho_{[x_1, x_2]} \log_2 \rho_{[x_1, x_2]}]$ for the noise averaged reduced density matrix $\rho_{[x_1, x_2]}$, is because in the long time limit $\rho(t)$ turns into an infinite temperature state. Therefore the EE of the block of spins between x_1 and x_2 would be trivial and will not capture any effects of noise on the entanglement dynamics.

To compute $\langle S_{ent}^\eta(t) \rangle_\eta$, we use the fact that the quantum state of each trajectory of the SSE Eq. (9), is Gaussian [36]. Therefore the dynamics of each trajectory can be obtained by computing the evolution of the two point correlation functions:

$$\mathcal{C}^\eta(t) = \begin{bmatrix} \hat{1} - C^\eta(t) & F^\eta(t)^\dagger \\ F^\eta(t) & C^\eta(t) \end{bmatrix}. \quad (24)$$

where C and F are defined as:

$$C_{i,j}^\eta(t) = \langle c_i^\dagger(t) c_j(t) \rangle, F_{i,j}^\eta(t) = \langle c_i^\dagger(t) c_j^\dagger(t) \rangle. \quad (25)$$

The numerical scheme that we use for obtaining $\mathcal{C}^\eta(t)$ discretizes time in steps of δt . The n^{th} instant is given as

$t_n = (n-1)\delta t$ with $n = 1, 2, \dots$ and $\delta t \ll \min\{h^{-1}, \kappa^{-1}\}$. The correlation matrix \mathcal{C}_n^η at time step t_n is computed from the correlation matrix \mathcal{C}_{n-1}^η at time t_{n-1} by:

$$\mathcal{C}_n^\eta = e^{-iM^\eta \delta t} \mathcal{C}_{n-1}^\eta e^{iM^\eta \delta t}, \quad (26)$$

$$M^\eta = M_0 + \sqrt{\kappa} \eta(t_{n-1}) \mathcal{L}.$$

The operator $e^{-iM^\eta \delta t}$ can be computed effiecntly via Trotterization:

$$e^{-iM^\eta \delta t} \approx e^{-i\sqrt{\kappa} \eta(t_{n-1}) \frac{\delta t}{2}} e^{-iM_0 \delta t} e^{-i\sqrt{\kappa} \eta(t_{n-1}) \mathcal{L} \frac{\delta t}{2}}.$$

Having started in a Gaussian state, we compute the correlation matrix for the initial state $\mathcal{C}(0)$ and use it as an initial condition for the above mentioned numerical time evolution scheme. In case of a gaussian state, the entanglement entropy is given by [47–49]

$$S_{ent}^\eta(t) = -\sum_p [\lambda_p \log_2 \lambda_p]. \quad (27)$$

where $\{\lambda_p\}$ are the eigenvalues of the matrix

$$\mathcal{C}_{sub}^\eta(t) = \begin{bmatrix} (\hat{1} - C^\eta(t))_{i,j=x_1}^{x_2} & ((F^\eta(t))^\dagger)_{i,j=x_1}^{x_2} \\ (F^\eta(t))_{i,j=x_1}^{x_2} & (C^\eta(t))_{i,j=x_1}^{x_2} \end{bmatrix}. \quad (28)$$

The $(A)_{i,j=x_1}^{x_2}$ is a matrix which contains all the elements of matrix A , between $x_1 \leq i \leq x_2$ and $x_1 \leq j \leq x_2$.

We then compute $\langle S_{ent}^\eta(t) \rangle_\eta$ by averaging $S_{ent}^\eta(t)$ over various noise realisations.

To compare with [36], we also investigate the following fluctuation correlation function:

$$\Delta_{LR}^\eta = \langle \hat{N}_R \hat{N}_L \rangle - \langle \hat{N}_L \rangle \langle \hat{N}_R \rangle, \quad (29)$$

where \hat{N}_L represents the total number of fermions on l sites to the left of the impurity (we fix $l = 5$)

$$\hat{N}_L \equiv \sum_{i=-l}^{-1} \hat{n}_i. \quad (30)$$

and \hat{N}_R is defined analogously. Eq. (29) serves as a proxy for transport properties across the dissipative site and we use it to probe the correlation formation in non-equilibrium steady state forming around the impurity (see Fig. 2b). Using the correlation matrix (28), we can evaluate (29) as follows

$$\Delta_{LR}^\eta = \sum_{i=-l}^{-1} \sum_{j=1}^l (-|C_{ij}^\eta(t)|^2 + |F_{ij}^\eta(t)|^2). \quad (31)$$

B. Entanglement dynamics in the Gaussian white noise limit.

In this subsection we present two key features of EE dynamics that our numerical simulations reveal. In particular we focus on the half chain entanglement entropy for spin between $x_1 = 0$ and $x_2 = L$. First, we observe an expected linear growth of the EE [50] and second, we observe a non-monotonous behaviour of the EE's first derivative as a function of the coupling κ to the stochastic field (see Fig. 2a).

Both observations can be qualitatively explained with the quasi-particle picture [50, 51], which has been also successfully applied in the XX chain subject to global noise [46]. In our case, the impurity emits highly entangled quasi-particle pairs which travel in opposite directions and entangle any two spatial sites at which the pair arrives simultaneously; this gives the usual linear growth in time of the EE. In the thermodynamic limit the light cone that originates at the driven site will take an infinite time to reach the edge of the system, hence the EE of the block we are studying will increase unboundedly.

The non-monotonous behaviour of the rate of change of EE can be explained by understanding the competition between the hopping strength of quasi-particles and the rate κ which controls the production of quasi-particles. Let us consider two limiting cases. In the Zeno regime ($\kappa \gg 1$) most of the quasi-particles produced remain trapped near the impurity site as the hopping term is too small to transport them through the system. In the heating phase ($\kappa \ll 1$) the impurity produces a very small number of quasi-particle pairs (see Fig. 3a) as compared to the Zeno-regime and they spread across the system.

When we increase κ in the heating side, we observe an increase in the number of quasi-particles (see Fig. 3a) which easily spread throughout the system because of relatively strong hopping term and hence take part in entangling the left and right halves of the system. This results in the increase of \dot{S}_{ent} (see Fig. 2a). However, when $\kappa \sim 1$ inspite of having a large number of quasi-particles available for entangling the two halves of the system, we observe a stagnation in the value of \dot{S}_{ent} . The value of \dot{S}_{ent} reduces on further increase in κ . This happens as a consequence Zeno crossover which kicks in when $\kappa \sim 1$ and can be seen as a transition from the regime where quasi-particles are delocalised throughout the system, to a regime where they are mostly trapped near the impurity site (see Fig. 3b). As a consequence, inspite of having a very large number of quasi-particles as compared to the heating regime, we see a decline of \dot{S}_{ent} in the Zeno regime, because most of the quasi-particles will be unable to escape from a neighbourhood of the impurity.

C. Effect of a finite noise correlation time

In this subsection we discuss the effects of finite correlation time τ of the noise on the velocity of entanglement spreading in the heating and Zeno regimes. In the heating regime, the velocity of entanglement spreading reduces with an increase in τ (see Fig. 2a). This is due to the reduction in the total number of injected quasi-particle pairs (see Fig. 3a) that can participate in entanglement growth.

In the Zeno regime $\kappa \gg 1$ we observe the exact opposite: the suppression of velocity of entanglement spreading reduces with increasing τ . This is attributed to the fact that as τ increases, the trapping of quasi-particles near the impurity site becomes less effective (cf. with Fig. 3b). This allows more quasi-particle pairs to participate in entangling the sub-system $[0, L]$ with its complement and hence we observe larger values of \dot{S}_{ent} as τ increases. In other words, the tunnelling across the dissipative impurity becomes increasingly more coherent at larger τ and the Zeno effect is expected to attenuate; this explains a shift of the Zeno crossover to larger values of κ (cf. with Fig. 2a and 2b). We carried numerical simulations for larger values of τ and we could not find a critical value of τ where the Zeno effect completely disappears; the only net effect of a dissipative impurity with finite correlation time is to extend the heating phase to larger κ .

Notice that there is a minor contribution to enhancement of \dot{S}_{ent} in the Zeno regime from increased number of quasi-particle pairs for finite τ as compared to $\tau = 0$. However, the difference in number of quasi-particle pairs between $\tau > 0$ and $\tau = 0$ is much smaller than what is observed in the heating regime. Also, the results presented in this section for the $\gamma = 0$ case, qualitatively remain the same for $\gamma > 0$. We carried out simulations

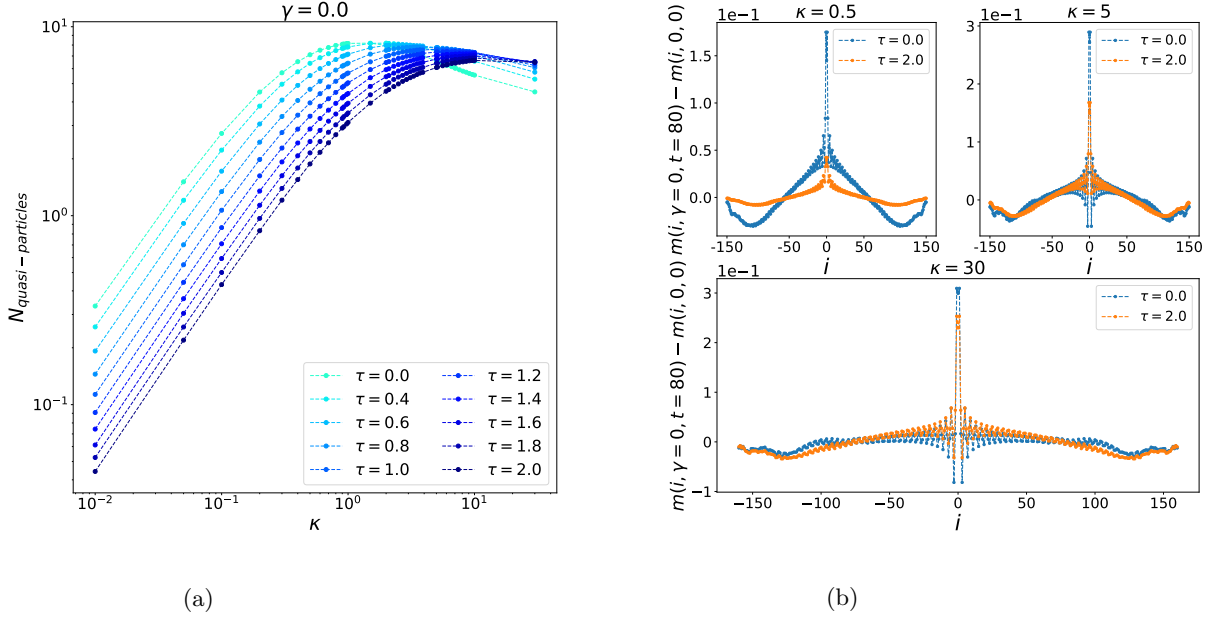


FIG. 3: (a) Number of quasi-particles produced, $N_{qp} = \sum_i |\langle m^\eta(i, \gamma = 0, t) \rangle_\eta - \langle m^\eta(i, \gamma = 0, 0) \rangle_\eta|$ at $t = 80$, as a function of κ . In the heating regime, N_{qp} grows algebraically with κ while in the Zeno regime, it remains constant or decreasing. (b) Local magnetisation profile ($m(i, \gamma, t) = \langle m^\eta(i, \gamma, t) \rangle_\eta$) for $\tau = 0$ and $\tau = 2$. In the heating regime ($\kappa = 0.5$), most of the injected quasi-particle pairs result in the formation of a ballistic density front which starts from the impurity site and propagates towards the edge of the system, entangling $[0, L]$ with its complement where as, in the Zeno regime ($\kappa = 30$) the majority of injected quasi-particles appear to be localised near the impurity. This remains true for both $\tau = 0$ and $\tau = 2$ cases. In the Zeno regime ($\kappa = 30$) we observe that, for $\tau = 2$, the trapping is attenuated with respect to $\tau = 0$. This reflects in relative difference of the peak value of the local magnetisation near the impurity, observed in the two cases. These results were computed using the same method and parameters as discussed in Fig. 2

to verify this claim.

V. PERSPECTIVES

The observation that the entanglement entropy can detect the crossover from the heating to the Zeno regime, opens to the perspective of connecting the field of dissipative impurities with a new class of non-equilibrium entanglement transitions recently studied in random hybrid circuits. In that context, the competition of unitary entangling gates with projective measurements results in a Zeno effect separating an area law and volume law phases, upon reducing the measurement rate [52]. Developing platforms where dissipative impurities can expose similar effects, could result in experimental proposals for detecting entanglement transitions using, for instance, cold atoms [53].

We believe that our results hold a certain level of generality. The local dissipative channel studied here contains, for finite anisotropy ($\gamma \neq 0$), both heating, pump and loss effects (cf. Eq. (19)), therefore, we expect that solving the problem with incoherent spin losses would

lead to qualitatively similar results for the dynamics of the entanglement entropy. From a technical side, it could be interesting to apply methods for the exact solution of boundary driven problems [23–29] in order to extend our results to interacting versions of the free fermion model considered here. A relevant question is the possibility to morph the Zeno effect from a crossover into a sharp transition in the presence of interactions, and inspect the impact of a driving noise with finite correlation time on such transition. Our current efforts are directed in this direction.

ACKNOWLEDGEMENTS

We thank B. Buca for constructive discussions. JM gratefully acknowledges P. Dolgirev, D. Sels and E. Demler for collaborations on related topics. AC thanks R. Singh for helpful discussions and for the computational resources. The support and the resources provided by ‘PARAM Shivay Facility’ under the National Supercomputing Mission, Government of India at the Indian Institute of Technology, Varanasi are gratefully acknowledged.

-
- [1] I. Affleck, [arXiv:0809.3474 \[cond-mat\]](#) (2009), [arXiv:0809.3474](#).
- [2] G. D. Mahan, *Many-particle physics* (Springer Science & Business Media, 2013).
- [3] D. A. Zezyulin, V. V. Konotop, G. Barontini, and H. Ott, *Phys. Rev. Lett.* **109**, 020405 (2012).
- [4] G. Barontini, R. Labouvie, F. Stubenrauch, A. Vogler, V. Guarrera, and H. Ott, *Phys. Rev. Lett.* **110**, 035302 (2013).
- [5] B. Misra and E. G. Sudarshan, *J. Math. Phys.* **18**, 756 (1977).
- [6] W. M. Itano, D. J. Heinzen, J. Bollinger, and D. Wineland, *Phys. Rev. A* **41**, 2295 (1990).
- [7] P. Facchi and S. Pascazio, *Phys. Rev. Lett.* **89**, 080401 (2002).
- [8] A. Kofman and G. Kurizki, *Phys. Rev. A* **54**, R3750 (1996).
- [9] A. Kofman, G. Kurizki, and T. Opatrny, *Phys. Rev. A* **63**, 042108 (2001).
- [10] A. Kofman and G. Kurizki, *Nature* **405**, 546 (2000).
- [11] H. Fröml, A. Chiocchetta, C. Kollath, and S. Diehl, *Phys. Rev. Lett.* **122**, 040402 (2019).
- [12] M. Lebrat, S. Häusler, P. Fabritius, D. Husmann, L. Corman, and T. Esslinger, *Phys. Rev. Lett.* **123**, 193605 (2019).
- [13] L. Corman, P. Fabritius, S. Häusler, J. Mohan, L. H. Dogra, D. Husmann, M. Lebrat, and T. Esslinger, *Phys. Rev. A* **100**, 053605 (2019).
- [14] F. Tonielli, R. Fazio, S. Diehl, and J. Marino, *Phys. Rev. Lett.* **122**, 040604 (2019).
- [15] M. Schiro and O. Scarlatella, *The Journal of chemical physics* **151**, 044102 (2019).
- [16] F. Tonielli, N. Chakraborty, F. Grusdt, and J. Marino, *Phys. Rev. Research* **2**, 032003 (2020).
- [17] C. Baals, A. G. Moreno, J. Jiang, J. Benary, and H. Ott, [arXiv preprint arXiv:2012.11487](#) (2020).
- [18] A. Biella and M. Schiró, [arXiv preprint arXiv:2011.11620](#) (2020).
- [19] A. Sartori, J. Marino, S. Stringari, and A. Recati, *New Journal of Physics* **17**, 093036 (2015).
- [20] T. Yoshimura, K. Bidzhiev, and H. Saleur, *Phys. Rev. B* **102**, 125124 (2020).
- [21] A. Khedri, A. Štrkalj, and O. Zilberberg, [arXiv preprint arXiv:2012.04628](#) (2020).
- [22] T. Maimbourg, D. M. Basko, M. Holzmann, and A. Rosso, [arXiv preprint arXiv:2009.11784](#) (2020).
- [23] B. Žunkovič and T. Prosen, *J. Stat. Mech.: Theory Exp.* **2010**, P08016 (2010).
- [24] M. Žnidarič, *Phys. Rev. E* **83**, 011108 (2011).
- [25] T. Prosen, *J. Phys. A* **48**, 373001 (2015).
- [26] M. Žnidarič, *Phys. Rev. E* **92**, 042143 (2015).
- [27] W. Berdanier, J. Marino, and E. Altman, *Phys. Rev. Lett.* **123**, 230604 (2019).
- [28] B. Buča, C. Booker, M. Medenjak, and D. Jaksch, *New Journal of Physics* **22**, 123040 (2020).
- [29] V. Alba and F. Carollo, [arXiv preprint arXiv:2103.05671](#) (2021).
- [30] H. Fröml, C. Muckel, C. Kollath, A. Chiocchetta, and S. Diehl, *Phys. Rev. B* **101**, 144301 (2020).
- [31] P. Krapivsky, K. Mallick, and D. Sels, *J. Stat. Mech.: Theory Exp.* **2019**, 113108 (2019).
- [32] T. Wasak, R. Schmidt, and F. Piazza, *Phys. Rev. Research* **3**, 013086 (2021).
- [33] S. Wolff, A. Sheikhan, S. Diehl, and C. Kollath, *Phys. Rev. B* **101**, 075139 (2020).
- [34] M. T. Mitchison, T. Fogarty, G. Guarnieri, S. Campbell, T. Busch, and J. Goold, *Phys. Rev. Lett.* **125**, 080402 (2020).
- [35] T. Müller, M. Gievers, H. Fröml, S. Diehl, and A. Chiocchetta, [arXiv preprint arXiv:2105.01059](#) (2021).
- [36] P. E. Dolgirev, J. Marino, D. Sels, and E. Demler, *Phys. Rev. B* **102**, 100301 (2020).
- [37] F. Franchini, *An Introduction to Integrable Techniques for One-Dimensional Quantum Systems* (Springer International Publishing, 2017).
- [38] C. Gardiner and P. Zoller, *Quantum noise: a handbook of Markovian and non-Markovian quantum stochastic methods with applications to quantum optics* (Springer Science & Business Media, 2004).
- [39] K. Jacobs and D. A. Steck, *Contemporary Physics* **47**, 279 (2006), <https://doi.org/10.1080/00107510601101934>.
- [40] T. Lancaster and S. J. Blundell, *Quantum Field Theory for the Gifted Amateur* (Oxford Scholarship Online, 2014).
- [41] G. B. Mbeng, A. Russomanno, and G. E. Santoro, [arXiv preprint arXiv:2009.09208](#) (2020).
- [42] P. Calabrese, F. H. L. Essler, and M. Fagotti, *Journal of Statistical Mechanics: Theory and Experiment* **2012**, P07016 (2012).
- [43] H. Rieger and F. Iglói, *Phys. Rev. B* **84**, 165117 (2011).
- [44] B. Bertini and M. Fagotti, *Journal of Statistical Mechanics: Theory and Experiment* **2015**, P07012 (2015).
- [45] M. Fagotti, *Journal of Statistical Mechanics: Theory and Experiment* **2014**, P03016 (2014).
- [46] X. Cao, A. Tilloy, and A. De Luca, *SciPost Physics* **7** (2019), [10.21468/SciPostPhys.7.2.024](https://doi.org/10.21468/SciPostPhys.7.2.024).
- [47] S. Nandy, A. Sen, A. Das, and A. Dhar, *Phys. Rev. B* **94**, 245131 (2016).
- [48] L. Amico, R. Fazio, A. Osterloh, and V. Vedral, *Rev. Mod. Phys.* **80**, 517 (2008).
- [49] S. Lorenzo, J. Marino, F. Plastina, G. M. Palma, and T. J. G. Apollaro, *Scientific Reports* **7**, 5672 (2017).
- [50] P. Calabrese and J. Cardy, *Journal of Statistical Mechanics: Theory and Experiment* **2016**, 064003 (2016).
- [51] P. Calabrese and J. Cardy, *Journal of Statistical Mechanics: Theory and Experiment* **2005**, P04010 (2005).
- [52] Y. Li, X. Chen, and M. P. A. Fisher, *Phys. Rev. B* **98**, 205136 (2018).
- [53] R. Islam, R. Ma, P. M. Preiss, M. E. Tai, A. Lukin, M. Rispoli, and M. Greiner, *Nature* **528**, 77 (2015).